

## PHASE EVOLUTION IN AN MCrAlY COATING DURING HIGH TEMPERATURE EXPOSURE

C. Costa<sup>a</sup>, E. Barbareschi<sup>b</sup>, P. Guarnone<sup>b</sup>, G. Borzone<sup>a,\*</sup>

<sup>a</sup>Department of Chemistry and Industrial Chemistry (DCCI), University of Genoa, Genoa, Italy

<sup>b</sup>Ansaldo Energia S.p.A. Corso Perrone, Genoa, Italy

(Received 05 July 2012; accepted 14 October 2012)

### Abstract

*MCrAlY (M = Ni and/or Co) coating systems are often applied on gas turbine blades and vanes to withstand the challenges of severe conditions. During service MCrAlY coatings are subjected to microstructural transformations that can be an indication of components service temperatures. The development of indirect methods to measure this parameter is of great concern in the gas turbine “world” due to the impossibility of direct measurements.*

*In the present work the evolution of an MCrAlY coating applied on René80 by LPPS (Low Pressure Plasma Spray) technique has been studied in order to verify if it was possible to identify a microstructural indicator of the service temperature. The specimens were exposed for different lengths of time at test temperatures of 700 - 800 - 900°C in order to characterize the phase evolution with time and temperature. Selective etching was employed for optical metallographic investigation. Scanning Electron Microscopy (SEM) observation combined with Electron Backscattered Diffraction (EBSD) and Energy Dispersive Spectroscopy (EDS) showed that the coating is composed of a  $\gamma$ -Co matrix,  $\beta$ -AlNi,  $\sigma$ -(Cr, Co), Cr carbide and Y-rich phases. Among these phases, the sigma phase resulted in a temperature – composition dependence that can be a useful tool for evaluating the local service temperature and modelling the residual lifetime.*

*Keywords: MCrAlY coating; Phase evolution; Sigma phase; Service temperature.*

### 1. Introduction

Nowadays, reliability of structural materials in gas and oil-fired gas turbines is a matter of concern considering the continuous push towards higher turbine inlet temperature [1]. Combining strength-at-temperature capabilities and resistance against environmental attack is achieved through the use of Ni base superalloys with protective coatings [2]. This oxidation protection task is generally fulfilled by an overlay coating, a metallic layer based on modified MCrAlY (M = Ni and/or Co) corrosion resistant alloys [3].

Within the MCrAlY family, it is possible to identify two groups of coating referring to their chemical composition: Ni-based alloys, with high Al content, fulfilling performance requirements against oxidation, and Co or Co-Ni-based alloys with high Cr content, particularly efficient against hot corrosion. Frequently active elements such as Y, Si and Hf (with high oxygen affinity) are alloyed, thus improving scale adherence; added quantities of refractory elements (mainly Ta and Re) also have a beneficial effect on oxidation resistance [4, 5].

The major phases of MCrAlY-type coatings are the austenitic matrix,  $\gamma$ -Ni (Co, Cr) or  $\gamma$ -Co (Ni, Cr) having a cF4-Cu type structure, and  $\beta$ -AlNi phase (cP2-CsCl type) which is responsible for resistance to environmental

conditions since it acts as a source of Al, an element capable of forming a protective, stable and slow-growing Al<sub>2</sub>O<sub>3</sub> scale layer on the component surface.

The natural evolution of an MCrAlY coating foresees chemical and microstructural modifications due to high temperature exposure,  $\beta$ -phase consumption by coating oxidation, and element interdiffusion at the internal (coating/superalloys) and external (coating/environment) interfaces where the TGO (Thermally Grown Oxide) grows. At these interfaces a depletion layer of the  $\beta$ -phase appears dividing the coating in three zones. From the base material to the TGO, the first one is the internal depletion zone (IDZ); the second is the central area and the third is the outer depletion zone (ODZ).

Preferential oxidation of Al is at the base of protection against oxidation, and empirical dependences in defining coating lifetime at the usual operating temperatures have to take into account Al inward/outward diffusion conveyed by Al<sub>2</sub>O<sub>3</sub> oxide thickness variation, concentration profiles and volume fractions of residual  $\beta$ -phase inside the coating [6].

The complexity of processes activated by high temperature exposure still requires an enormous effort in the chemical composition and microstructure optimization. Prediction of the evolution and residual lifetime of the coating system rely on calculation and experimental results

---

\* Corresponding author: [gabriella.borzone@unige.it](mailto:gabriella.borzone@unige.it)

[7]. It was found that, below 1000°C, Cr-rich,  $\sigma$ -(Cr, Co or Re) and  $\gamma'$ -Ni<sub>3</sub>Al secondary phases may be detected [8]. Critically assessed thermodynamic and mobility databases are used to perform thermodynamic calculation in the CALPHAD framework on simplified system related to the Ni-Cr-Al ternary system. Kinetic information is merged by the introduction of interdiffusion coefficient in order to obtain reliable diffusion paths and accurate simulation of microstructural evolution [8 - 11].

The actual composition, phase and microstructure modifications are experimentally evaluated after oxidation/corrosion tests or high temperature exposure for extended periods. This full characterization enables the development of an evolution library that is useful as feedback in calculation and simulation processes or as a source of empirical parameters defining a direct relationship between data and working temperature [12, 13].

In NiCoCrAlY coatings, Co is reported to increase the stability of the  $\sigma$  phase leading to the appearance of a four-phase field ( $\gamma+\gamma'+\sigma+\beta$ ) [6, 8, 10]. Above a certain concentration level, in NiCoCrAlY and CoNiCrAlY coatings, it seems that Co suppresses the  $\gamma'$  formation. Moreover in Re containing coating,  $\sigma$ , Y- and Cr-rich phases are promoted [9].

After longer oxidation time, a Cr-rich layer, identified as  $\alpha$ -Cr, accumulate at the alloy / thermally grown oxide (TGO) interface; together with the Y precipitates, these phases are considered to play a role in improving the oxidation performance of the coating [14].

In the present work an experimental approach has been carried out to investigate the phase evolution of a CoNiCrAlY coating applied by Low Pressure Plasma Spray (LPPS) on a René 80 substrate during high temperature exposure. The aim of this study was to investigate the thermodynamic stability of secondary phases, focusing on the experimental microstructural and chemical evolution of the  $\sigma$ -(Cr, Co) phase.

## 2. Experimental

The evolution of an MCrAlY coating (30%Ni, 28%Cr, 8%Al, 0.6%Y, 0.7%Si, balance cobalt) deposited by Low Pressure Plasma Spray (LPPS) on René 80 commercial alloy was studied as a function of time and temperature of exposure.

The investigated samples are listed in Table 1 and the

chemical composition of the superalloy is reported in Table 2. Isothermal annealing in air at three different temperatures (700, 800 and 900 °C ) were carried out for different exposure times (300, 500, 1000, 2000 and 3000 hours). After cooling in furnace, the specimens were mounted and polished using standard metallographic techniques. Selective etching was performed with the aim of identifying secondary phases by means of metallographic and optical analysis using Reichert MEF4M and Image Pro Plus v.6.2 software.

Field Emission Gun Scanning Electron Microscope (FEGSEM) Tescan Mira 3 equipped with EBSD Edax Hikari Camera and Edax Apollo X SDD detector systems was used to perform identification and subsequently crystallographic mapping of coating phases.

The morphology and compositions of various phases were studied using two different Scanning Electron Microscopes: Tescan Vega LSU equipped with Edax Apollo X SDD detector and Zeiss EVO 40 SEM (Carl Zeiss SMT Ltd., Cambridge) equipped with an INCA 300 Electron Probe MicroAnalysis (EPMA). Instrumental consistency was tested by repeating EDS analysis on the sample area and comparing phase composition results.

Accelerating voltage of 20 kV and a counting time of 30s were the setup conditions for chemical analysis on Tescan Vega LSU. Quantitative elaboration was done by ZAF (atomic number, absorption and fluorescence) standardless method.

Quantitative EDS analysis was carried out on Zeiss EVO 40 SEM using an acceleration voltage of 20 kV and a counting time of 50 s, using a cobalt standard in order to monitor beam current, gain and resolution of the spectrometer. Apparent compositions were finally corrected for ZAF effects using pure elements as standards.

The characterization of the samples was focused on phase identification and phase composition and divided in three steps:

1. Selective etching for optical observation of microstructural changes.
2. Phase identification by means of Electron

**Table 2.** Chemical composition of the René80 superalloy.

Superalloy	Composition/wt. %									
	Ni	Cr	Co	Ti	Al	Mo	W	C	B	Zr
René80	Bal.	14.1	9.5	5	3	4	4	0.17	0.015	0.063

**Table 1.** Test conditions (temperature and time of exposure at a specific temperature) of the investigated samples

Sample name	Deposition process	Base material	Test temperature /°C	Time test /h
MR7Xh	LPPS	René80	700	300-500-1000-2000-3000-5000
MR8Xh	LPPS	René80	800	300-500-1000-3000
MR9Xh	LPPS	René80	900	300-500-1000-2000-3000-5000
*The sample name contains the experimental information: M=MCrAlY on R=René80; 7, 8, 9 = test temperature 700, 800 ,900; Xh = hours of time exposure.				
LPPS = Low Pressure Plasma Spray				

Backscattered Diffraction (EBSD) patterns assignment.

3. Phase chemical evolution with temperature exposure through energy dispersive spectroscopy (EDS).

The reactivity of the phases containing Cr was tested with various chemical etching resulting in the best differentiation of the two Cr-rich phases with the Groesbeck solution. The etching tints  $\sigma$  phase a green-blue colour, while carbides appear outlined in white or sometimes brownish due to the etchant residual (see the darker and the brighter phase respectively in the greyscale image reported in figure 1) [15].

For the CoNiCrAlY coatings Toscano et al. [8] reported the following possible secondary phases:  $\beta$ -AlNi,  $\sigma$ -(Cr, Co) and Ni(Co)Y. Its presence was experimentally observed by X-Ray diffraction analysis by Toscano et al. [8], in

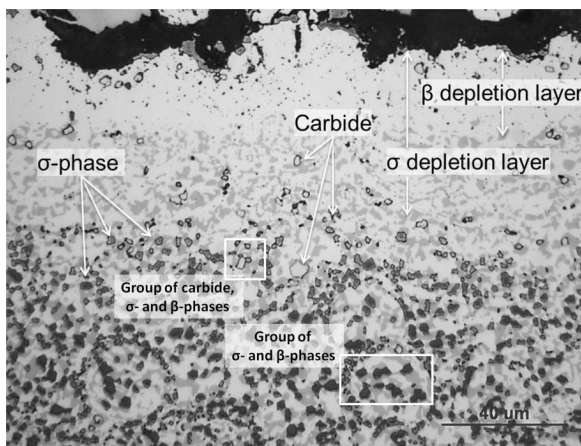


**Figure 1.** Micrograph of the sample MR93000h etched by Groesbeck solution with the indication of Cr-rich phases (carbide and sigma phase),  $\beta$ - and  $\sigma$ -depleted zones. The two insets show an example of areas where carbide and  $\sigma$ -phase grow close to the  $\beta$  phase.

agreement with the calculations of phase equilibria performed using commercially available software (ThermoCalc).

In the present work, EBSD investigations allowed the identification of two classes of Cr-rich phases,  $\sigma$  phase and Cr carbides (see figure 2).

In order to make possible the distinction of the  $\sigma$ -phase from the background and its chemical characterization, topographic information from a secondary electron (SE) signal was exploited. Moreover, a correspondence was identified between EBSD patterns of the sigma phase and two characteristic features in EDS spectra, readily attributable to this phase, which provides a suitable expedient for the SEM/EDS characterization.

### 3. Results

After Groesbeck etching, metallographic investigation of the secondary Cr-rich phases allowed an inspection on modification and distribution along the MCrAlY coating. The  $\sigma$ -phase is tinted in green-blue while carbides are white-brown; in the grayscale image  $\sigma$ -phase corresponds to darker or more etched precipitates. Figure 3 reports a collection of optical images from the etched coating for the two extreme temperatures. At 700°C a depleted area is observable only after 1000 hours and  $\sigma$ -phase is homogeneously distributed in the whole coating, while carbides are confined mainly at the internal and external interfaces with some sparse precipitates in the central area. During time exposure a coarsening effect modifies the shape of the particles from branched to somewhat round.

At 900°C, depleted areas become clearly visible from the beginning of the test time and a similar microstructural behaviour was detected during the time. For this temperature it is easier to identify the Cr-rich layer beneath the oxide [14]: it is made up of a string of carbide with a blocky morphology.

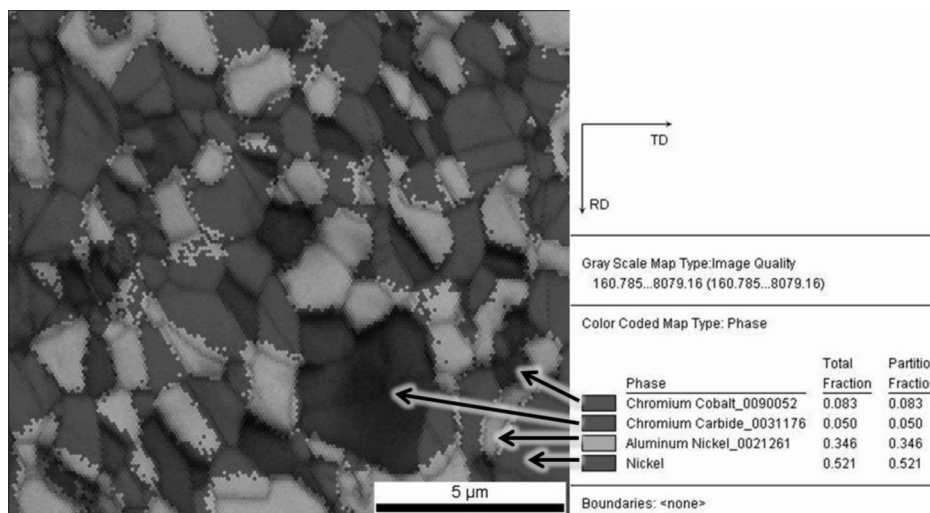


**Figure 2.** EBSD image quality map of an as-coated sample with superimposed a chemical filter with the legend for the identification of the different phases.

Electron Microscopy allowed the characterization of phases in the CoNiCrAlY coating. The  $\beta$  and  $\gamma$  phases were easily visible in the backscattered images due to their atomic contrast. For the identification of Cr-rich phases it was necessary to combine the different information from EBSD/SE/EDS techniques.

EBSD investigation was efficiently applied to identify all the phases in the CoNiCrAlY coating and to develop a characterization method for  $\sigma$ -phase that is merged into the  $\gamma$ -matrix because of the similar average atomic number.

One of the two Cr-rich phases detected by EBSD was identified as  $\sigma$ -(Cr, Co), with a tP30 -CrFe type crystal structure and a Cr content of about 48 wt%; the second one, having a higher Cr content, ( $\geq 70$  wt%) gave a more complex kikuchi patterns matching the cF116-Cr<sub>23</sub>C<sub>6</sub> type structure.

As mentioned above, the sigma phase is indistinct, due to its poor Z-contrast, with respect to the matrix and a simple SEM/BSE image identification is impossible but, since it is harder than the  $\gamma$  phase during polishing for microscopy observations it is emphasized in high relief (as Y-rich phase and carbide are). Secondary electron images can obtain this topographic information, which is not a univocal identification of the sigma phase but has to be confirmed by chemical results.

Figure 4A compares EDS spectra from the Y-rich phase, carbide and  $\sigma$ -phase, and shows several features characteristic for each phase as indicated by the arrows. For the sigma phase two specific signals were identified:

- a small peak of Si at 1.740 keV, which usually has an intensity similar to that of Al observed in the  $\sigma$ -phase at 1.490 keV.
- a tailed peak at 7.470 keV due to the overlapping of Ni

and Co signals.

Sigma phase does not dissolve a large quantity of yttrium (<1wt. %) while Y-precipitates have peaks of variable intensity at 1.920 keV corresponding to significant concentrations if compared to the coating average content. In the carbide the signal from Cr is big and dominant. Moreover, differentiation between carbide and sigma phase is possible by comparing the relative intensities of the Co and Ni peaks.

These peculiarities in the EDS spectra and the topography in the SEM/SE images due to different phase hardness (compare the SE image in figure 4B with the BSE image in figure 4C), allow the distinction of the  $\sigma$ -phase from the background and its chemical characterization.

EDS analysis has been carried out in order to characterize the phases in all three areas. It was proved that the coating zone has an influence on phase composition: the ODZ is not representative of the whole coating while the IDZ is sensitive to interdiffusing elements from the substrate (such as Ti, Mo and W); because of this, for general consideration, only the EDS analysis from the center of the metallic coating is considered.

In figure 5 the sigma phase composition as a function of time is reported. After 1000 hours, the annealing time does not affect significantly the composition of the phase, and only a modification in the amount of the phases formed in the coating was observed.

In addition, it was found that also the average composition for  $\beta$ - and  $\gamma$ -phase is quite constant at different temperatures. Information on carbide from the central area of the coating is partially lacking since the phase is not homogeneously distributed in the overall coating, and it

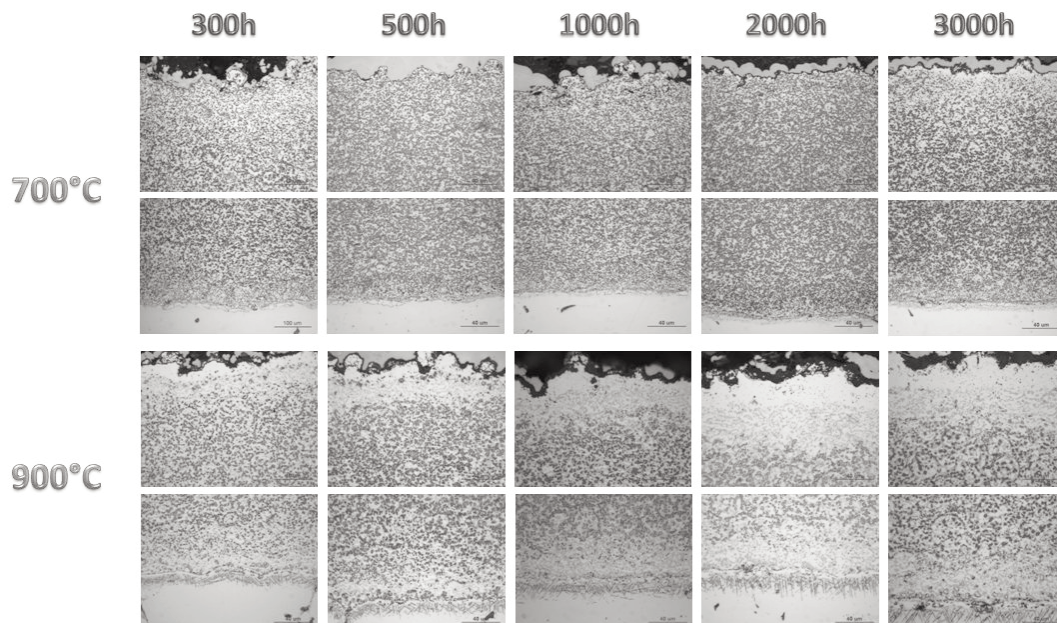


**Figure 3.** Micrograph collection of the samples etched by Groesbeck solution after different time of exposure at 700 and 900°C. To appreciate the microstructure in the whole coating, two images of the external and the internal part are reported for each time at 500 x.

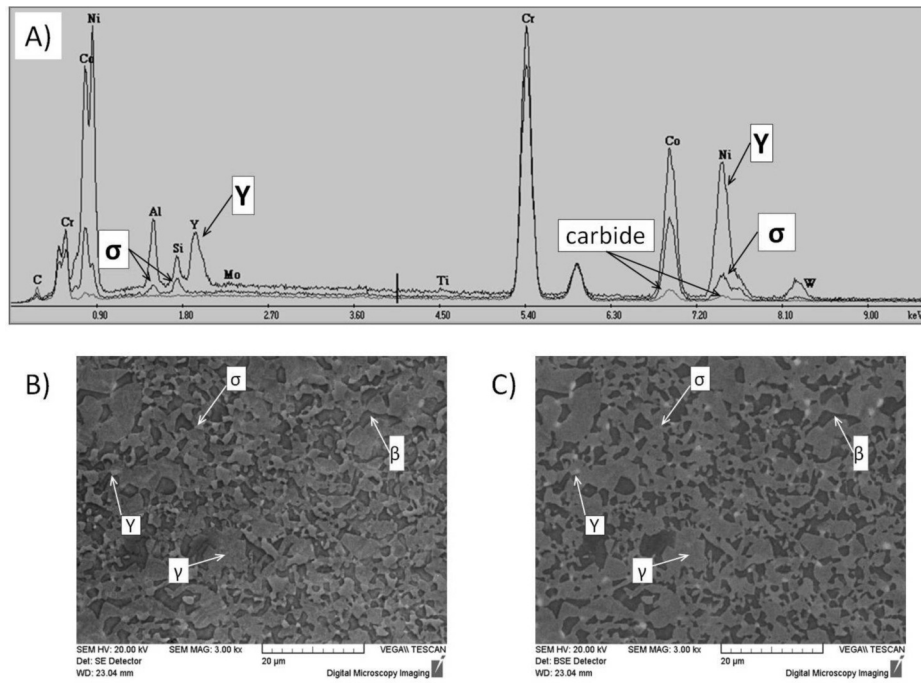


**Figure 4.** EDS analysis and micrographs of the CoNiCrAlY coating for MR93000h sample. A) Comparison of EDS spectra from secondary phases ( $\sigma$ , carbide and Y-rich phase). B) SE image; C) BSE image. Combining the information from different depth levels (SE image) and atomic number contrast (BSE image) it is possible to identify the  $\beta$ -,  $\gamma$ -,  $\sigma$ - phases and Y-precipitates.

covers just a small percentage of the area in the coating. Similar problems were encountered in the case of Y-precipitates:-

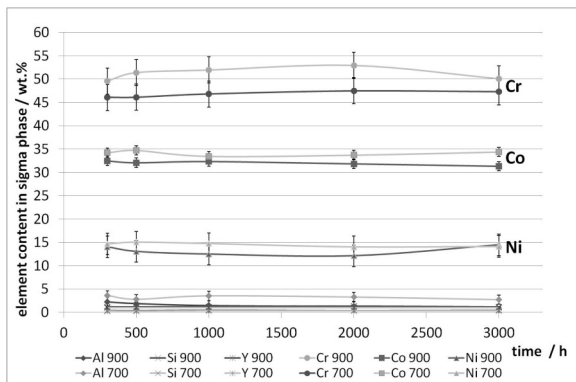


**Figure 5.** Element concentration at 700 and 900 °C in the  $\sigma$  phase as a function of time.

#### 4. Discussion

The  $\sigma$ -phase behaves in a different manner with respect to temperature, revealing an evident composition shift in its element content. Statistical tests were performed to evaluate element content in the sigma phase, and normal distributions calculated over a statistical number of analyses

for samples annealed for 3000h are shown in figure 6. There is a 5% probability of accepting or refusing the normality test, which is evaluated using the p-value. The smaller the p-value, the more strongly the test rejects the null hypothesis. For p-values greater than 0.05 the element content in the  $\sigma$  phase possesses a Gaussian trend. In the present case it is true for Si and Co at 700 °C; Co, Cr and Si at 800 °C and Si at 900 °C.

Considering Ni as a function of Cr content in the  $\sigma$ -phase, figure 7 shows the scattergram of experimental data. Ni and Cr are placed on the same line, which means the sum of these two elements is constant and increases with temperature. This relation denotes that the  $\sigma$ -phase dissolves higher quantities of Ni and Cr at higher temperature. Moreover, in the plot a cloudiness of points is visible for each temperature and implies that a more probable value of (Cr + Ni) sum exists as can be highlighted in a box plot reported in figure 8, by comparing hinge positions of the sum of these values for the three temperatures. Upper and lower limit of the boxes represent the 75th and 25th percentile respectively, the line crossing the box is the median, “whiskers” above and below each box specifies the spread of data at 99%, while the black square represents the average value and stars are outliers. Box position shows the temperature dependence of the most probable concentration value of these elements in the  $\sigma$ -phase. The (Cr + Ni) content is not constant when increasing the temperature from 700 to 900°C. This relationship is particularly interesting since it can be applied to predict local service

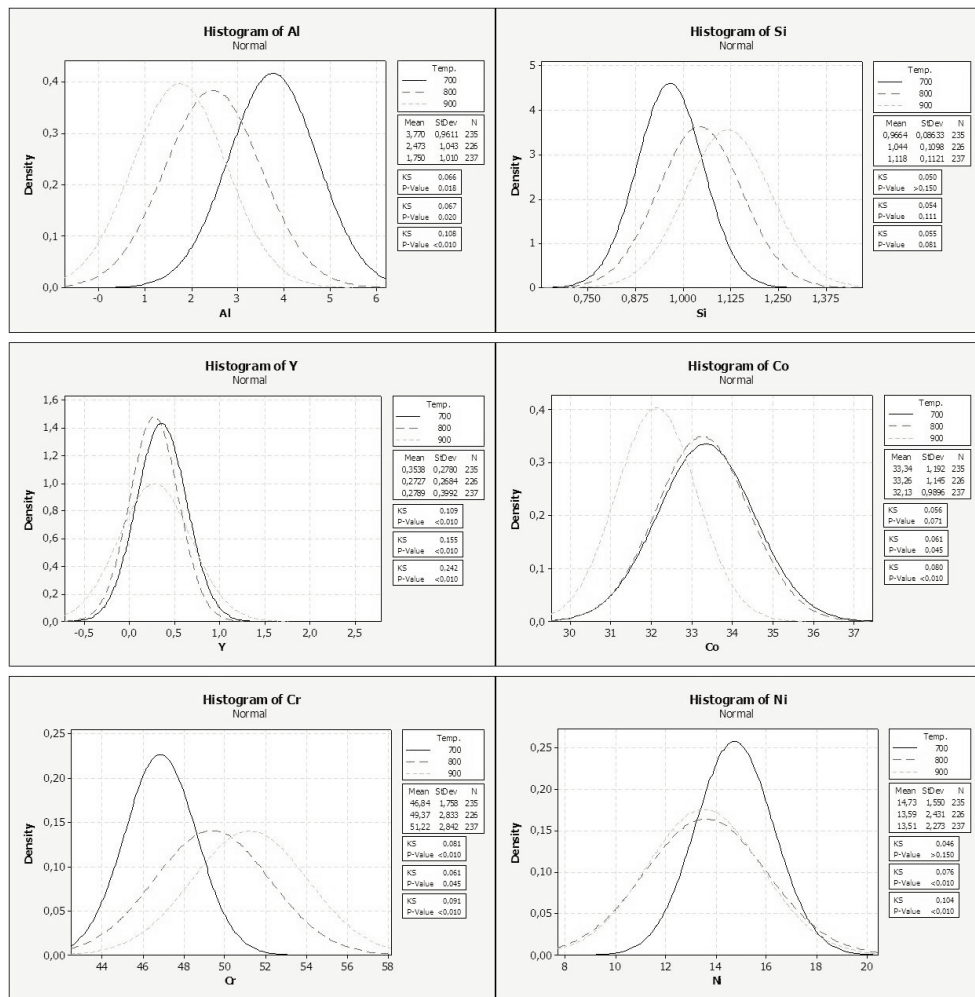


Figure 6. Normal distribution calculated on concentrations measured in a statistical number of  $\sigma$ -precipitates at the test temperatures. Data from samples exposed for 3000 h at 700 (—), 800 (- - -) and 900 °C.

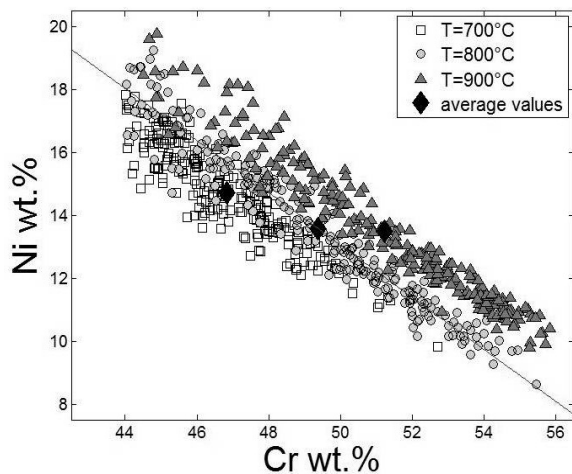


Figure 7. Scattergram of two of the components (Cr and Ni) measured in the  $\sigma$  phase by SEM-EDS analysis at different test temperatures 700, 800 and 900 °C.

temperature in blade samples. For the other elements there is no such clear separation in the scattergrams.

In the metallographic investigation it is worth noticing that as the temperature is increased to 900 °C the  $\sigma$ -phase is contained in the central area where the  $\beta$ -phase is still present, also creating depletion for this phase.

This can be clearly observed in the metallographic image shown in figure 1 for the sample MR93000h etched by Groesbeck.

Moreover the  $\sigma$ -distribution is not random and it grows close to the  $\beta$ -phase. Especially in the external area, group of  $\sigma$ -,  $\beta$ - and carbide precipitates were detected quite regularly. Similarly to what was observed by Na et al.[16] who considered the Cr-enriched area close to  $\gamma'$  as preferential nucleation site for the  $\sigma$ -phase, our experimental results suggest that the Cr-enriched area around  $\beta$ - phase acts as a nucleation site for sigma phase or carbides. Details on the quantitative results of the microstructural evolution of the  $\sigma$ -phase is in progress in our laboratory.

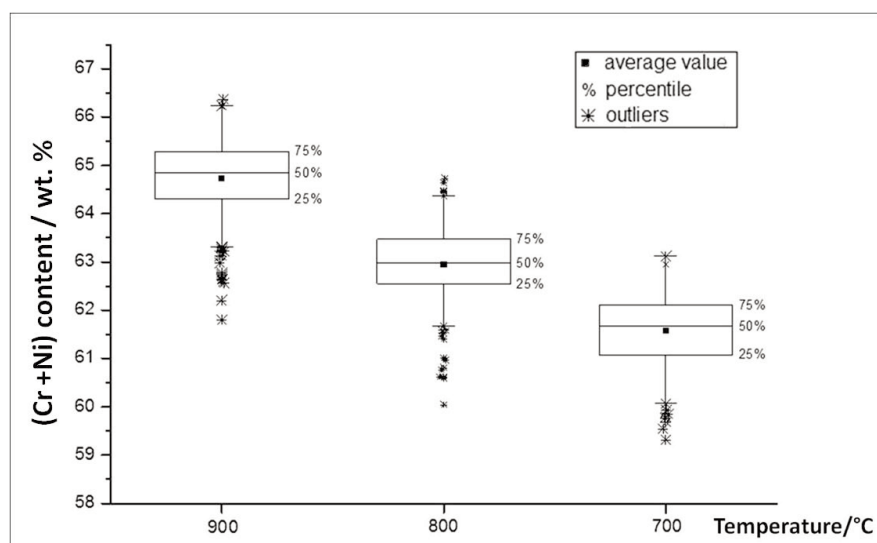


Figure 8. Box plot of the (Cr + Ni) content measured in the  $\sigma$ -phase at different temperatures.

## 5. Conclusions

In this study the microstructural phase evolution of the  $\sigma$ -(Cr, Co) phases of a CoNiCrAlY coating applied by Low Pressure Plasma Spray (LPPS) on a René 80 substrate subjected at different temperatures for different lengths of time has been experimentally investigated by microscope analyses. After annealing, the coating is composed of a  $\gamma$ -Co matrix,  $\beta$ -AlNi,  $\sigma$ -(Cr, Co), Cr carbide and Y-rich phases. None of these phases show a composition - exposure time relationship, with the exception of the sigma phase, for which a clear dependence of the (Cr+Ni) content with temperature was observed. The (Cr + Ni) content of the  $\sigma$ -phase increases with an increase in temperature.

The metallographic investigation highlighted the distribution of the carbides and the sigma phases with temperature and time along the coating, confirming the tendency of the  $\sigma$  phase to form close to the  $\beta$ -phase and showing the growth of a Cr-enriched area close to the oxide scale.

## Acknowledgments

Financial support for a PhD Grant from Regione Liguria DPU09DOTTOR - 3100 is gratefully acknowledged.

One of the Authors would like to thank Prof. Riccardo Leardi and Prof. Ivano Repetto of Genoa University for the useful discussions.

## References

- [1] M. M. Rahman, T. K. Ibrahim, A. N. Abdalla, *Int. J. Phys. Sci.*, 6 (14) (2011) 3539-3550.
- [2] S. Bose, *High Temperature Coatings*, Elsevier Science & Technology Books, Burlington (MA), 2007, p. 71.
- [3] J. R. Nicholls, N. J. Simms, W. Y. Chan, H. E. Evans., *Surf. & Coat. Tech.*, 149 (2-3) (2002) 236-244.
- [4] L. Huang, X.F. Sun, H.R. Guan, Z.Q. Hu, *Surf. Coat. Tech.*, 201 (2006) 1421-1425.
- [5] P. Y. Hou, *J. Am. Ceram. Soc.*, 86 (4) (2003) 660-668.
- [6] U. Täck, The influence of cobalt and rhenium on the behavior of MCrAlY coatings, PhD thesis, Technische Universität Bergakademie Freiberg, 2004, p. 81.
- [7] P. Krukovsky, K. Tadlya, A. Rybnikov, N. Mozhajskaia, I. Krukov, V. Kolarik, *Gas Turbines*, (Gurrappa Injeti), Sciyo, (2010), p. 325-346.
- [8] J. Toscano, A. Gil, T. Hüttel, E. Wessel, D. Naumenko, L. Singheiser, W.J. Quadackers, *Surf. Coat. Tech.* 202 (2007) 603-607.
- [9] D.R.G. Achar, R. Munoz-Arroyo, L. Singheiser, W.J. Quadackers, *Surf. Coat. Tech.*, 187(2-3) (2004) 272-283.
- [10] M. Kaka, J. M. Schoenung, *Surf. Coat. Tech.*, 205 (7) (2010) 2273-2280.
- [11] U. R. Kattner, C. E. Campbell, *Materials Science and Technology*, 25 (4) (2009) 443-459.
- [12] E. Barbareschi, A. Bonadei, A. Costa, P. Guarnone, E. Vacchieri, 9th Liège Conference: Materials for Advanced Power Engineering, September 27th - 29th, Liège, Belgium, 2010, p.76.
- [13] P. G. Krukovskii, K. A. Tadlya, *J. Eng. Phys. Thermophys.*, 30(3) (2007) 440-447.
- [14] H. Lan, P. Y. Hou, Z.-G. Yang, Y.-D. Zhang, C. Zhang, *Oxid. Met.*, 75 (1-2) (2011) 77-92.
- [15] G. F. Vander Voort, *Metallography: Principles and Practice*, McGraw-Hill Book Co., NY, 1984, ASM Intl, 1999, p. 752.
- [16] Y.S. Na, N.K. Park, R.C. Reed, *Scripta mater.*, 43 (2000) 585-590.